Supplementary Information: Lipid type doping of the sponge (L_3) mesophase

Christopher Brasnett[1, 5], Adam Squires[3], Andrew Smith[4], and Annela Seddon[1,2]

[1]School of Physics, University of Bristol, Tyndall Avenue, BS8 1FD, UK
[2]Bristol Centre for Functional Nanomaterials, School of Physics, University of Bristol, Tyndall Avenue, BS8 1FD
[3]Department of Chemistry, University of Bath, Bath, BA2 7AY, UK
[4]Diamond House, Diamond Light Source Ltd., Harwell Science and Innovation Campus, Fermi Ave., Didcot OX11 0DE, U.K.
[5]Present Address: Groningen Biomolecular Sciences and Biotechnology Institute, University of Groningen, Groningen, The Netherlands

S1 SAXS measurements

Lipid mesophases have characteristic scattering patterns, with Bragg peaks appearing in the following ratios:

- $x_{(n,L_\alpha)}$: $1 : 2 : 3 : \ldots$
- $x_{(n,H_{II})}$: $1 : \sqrt{3} : \sqrt{4} : \sqrt{7} : \ldots$
- $x_{(n,Q^D_{II})}$: $\sqrt{2} : \sqrt{3} : \sqrt{4} : \sqrt{6} : \sqrt{8} : \sqrt{9} : \ldots$

so that the lattice parameter can be calculated as:

$$a_{(n,L_\alpha)} = \frac{2\pi}{q_n} \times x_{(n,L_\alpha)}$$
$$a_{(n,H_{II})} = \frac{2}{\sqrt{3}}\frac{2\pi}{q_n} \times x_{(n,H_{II})}$$
$$a_{(n,Q^D_{II})} = \frac{2\pi}{q_n} \times x_{(n,Q^D_{II})}$$

The sponge mesophase has a broad peak, the centre (q_c) of which defines a bilayer-bilayer correlation length [1–3]:

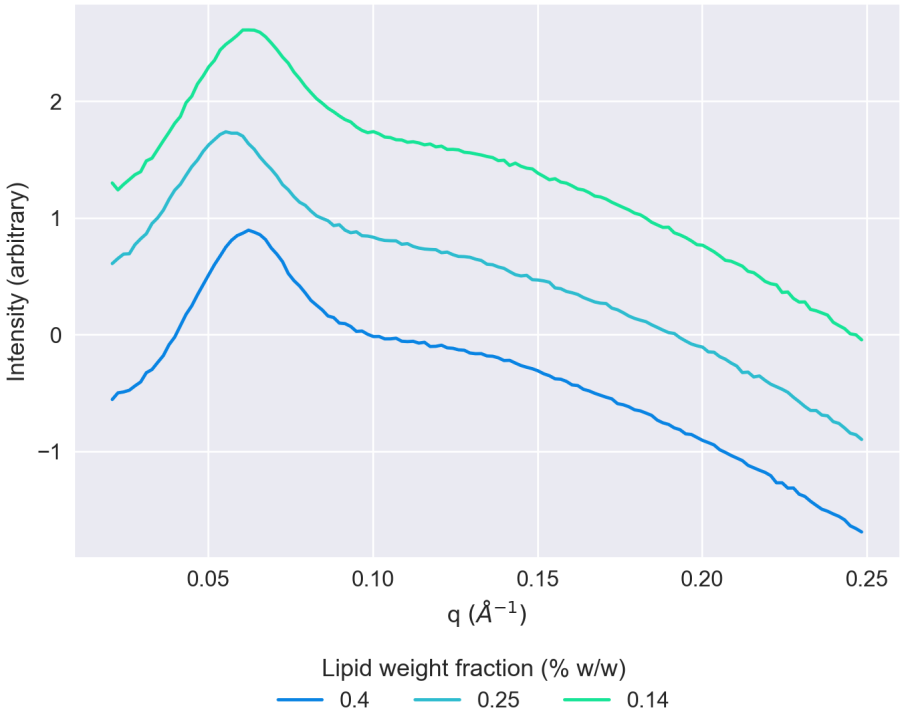

Figure S1: 1D SAXS patterns showing different weight ratios of lipid:solvent

$$a = \frac{2\pi}{q_c} \tag{1}$$

In the case of micelles, a core-shell ellipsoid form factor has a fringe after a first minima, which is known to correlate well with overall micelle size [4]. This is distinguishable from the broad scattering peak of the sponge mesophase, which does not exhibit such a minima. The centre of the peak, q_c can be used for this purpose:

$$d = \frac{2\pi}{q_c} \tag{2}$$

where d is the approximate micelle diameter.

S2 Excess solvent content

Our method of sample preparation differed from that of Cherezov et al. by using excess lyotropic conditions [5]. To ensure that our results were reproducible and

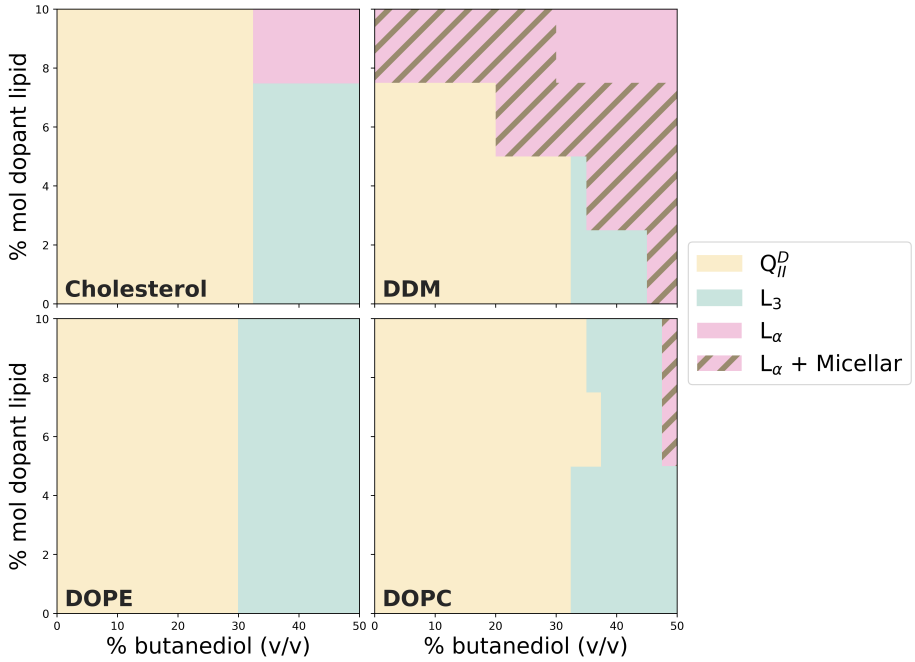

Figure S2: A summary phase diagram for the four single-doped systems studied in this work.

consistent, we measured the excess solvent mesophase behaviour using three different lipid:solvent weight ratios.

Samples were prepared by weighing a quantity of monoolein, and adding a corresponding weight of solvent at a fixed butanediol proportion of 40% v/v as required. The samples were mixed mechanically, transferred to an X-Ray capillary, sealed, and put through 3 freeze-thaw cycles to ensure equilibrium. They were measured for 600s in a q range of 0.015–0.65 $Å^{-1}$.

The azimuthal scattering patterns obtained and plotted in Figure S1 show that beyond an excess point, there is no substantial change in the mesophase behaviour of the monoolein/water/butanediol system between the different weight ratios. The correlation lengths measured for the 0.4, 0.25, and 0.14 %w/w systems were 101 Å, 111 Å, and 101 Å respectively.

S3 Summary phase diagram

In figure Fig. S2, we show a summary phase diagram of the single-doped monoolein systems studied in this work.

S4 Scattering patterns

S4.1 MO

Figure S3 shows integrated SAXS patterns for a pure monoolein system with varying proportions of butanediol in the solvent.

S4.2 Cholesterol

Figures S4 to S7 show integrated SAXS patterns for systems doped with 2.5% mol (Fig. S4), 5% mol (Fig. S5), 7.5% mol (Fig. S6), and 10% mol (Fig. S7) cholesterol.

S4.3 DOPE

Figures S8 to S11 show integrated SAXS patterns for systems doped with 2.5% mol (Fig. S8), 5% mol (Fig. S9), 7.5% mol (Fig. S10), and 10% mol (Fig. S11) DOPE.

S4.4 DOPC

Figures S12 to S15 show integrated SAXS patterns for systems doped with 2.5% mol (Fig. S12), 5% mol (Fig. S13), 7.5% mol (Fig. S14), and 10% mol (Fig. S15) DOPC.

S4.5 DDM

Figures S16 to S19 show integrated SAXS patterns for systems doped with 2.5% mol (Fig. S16), 5% mol (Fig. S17), 7.5% mol (Fig. S18), and 10% mol (Fig. S19) DDM.

S4.6 DOPG/cholesterol

Figures S20 to S21 show SAXS patterns for systems doped with 1% mol DOPG and 9% cholesterol (Fig. S20), and 3% mol DOPG and 7% cholesterol (Fig. S21). We note that the peaks in these systems are significantly broadend in comparison to other systems measured in this work, which is due to increased thermal fluctuations at large mesophase parameters. Therefore for clarity, we have indicated in Fig. S21 how the peaks were indexed during mesophase assignment.

S4.7 DOPG

Figures S22 to S24 show SAXS patterns for systems doped with 1% mol DOPG (Fig. S22), 3% mol DOPG (Fig. S23), and 5% mol DOPG (Fig. S24).

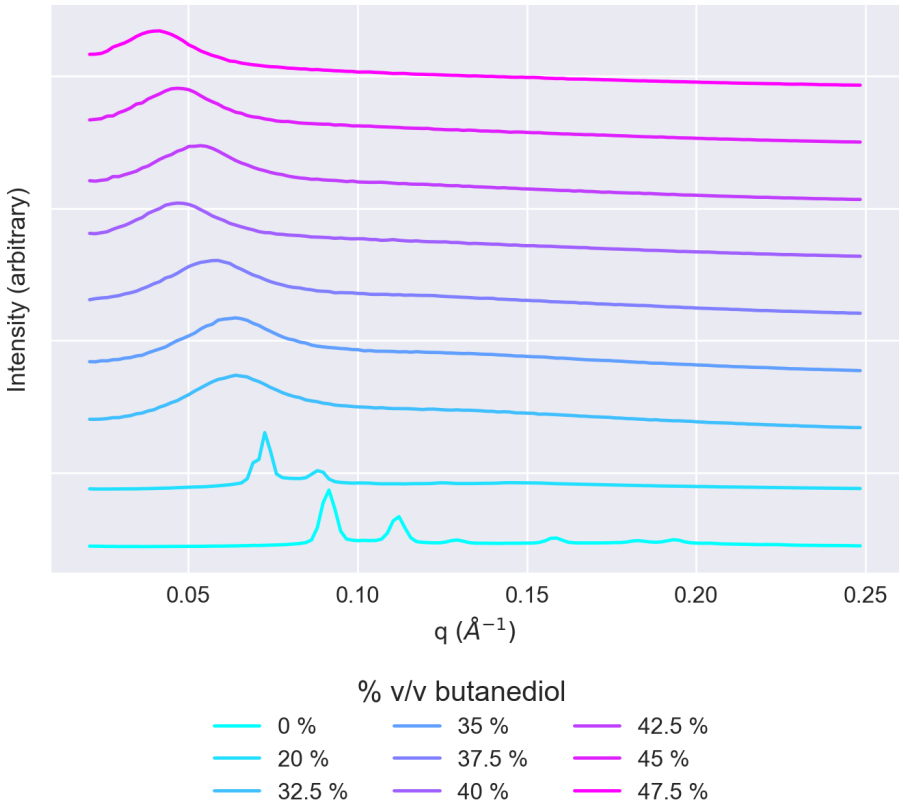

Figure S3: SAXS patterns for a pure MO system hydrated with a solvent of butanediol and water. The patterns are ordered with increasing butanediol solvent content from bottom to top.

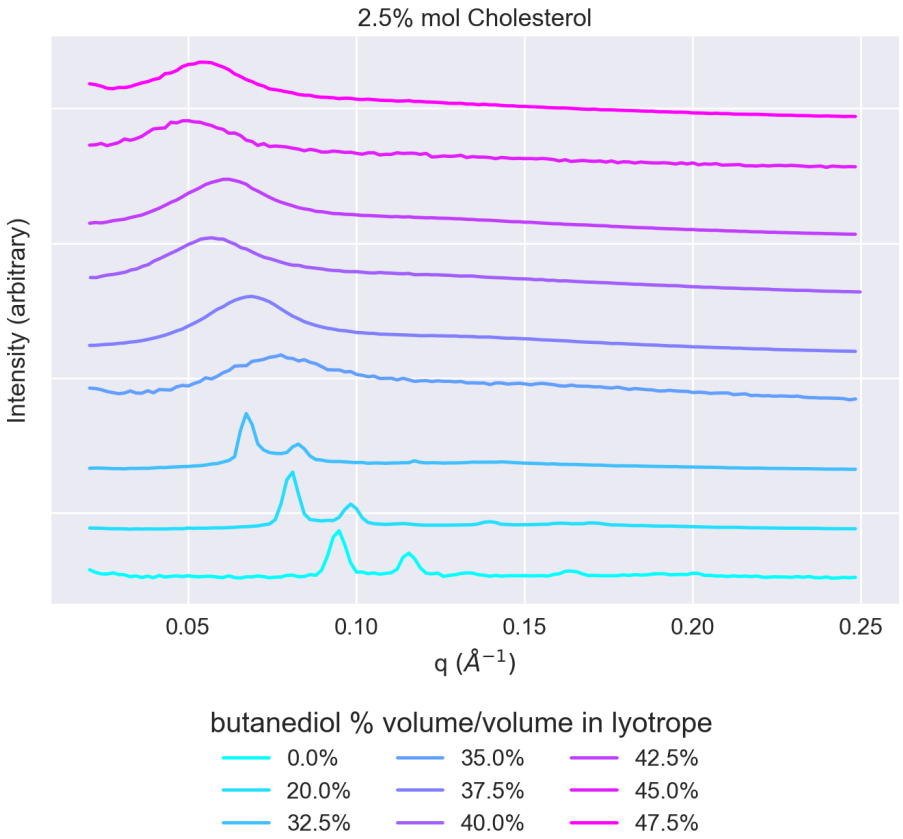

Figure S4: SAXS patterns for systems doped with 2.5% mol cholesterol. The patterns are ordered with increasing butanediol solvent content from bottom to top.

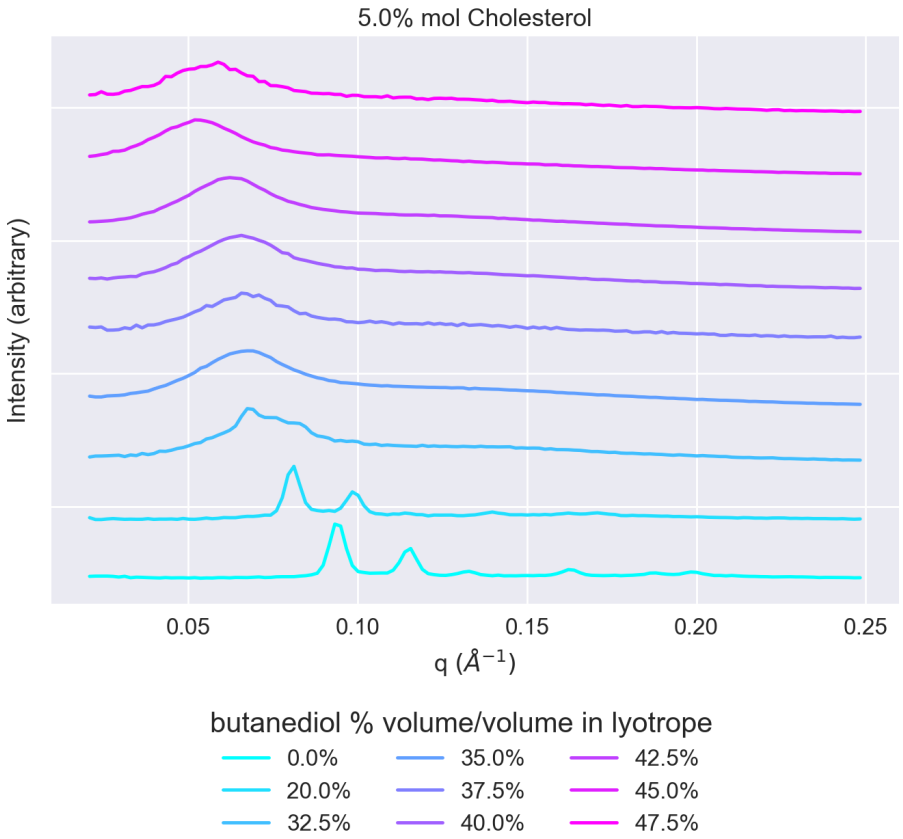

Figure S5: SAXS patterns for systems doped with 5% mol cholesterol. The patterns are ordered with increasing butanediol solvent content from bottom to top.

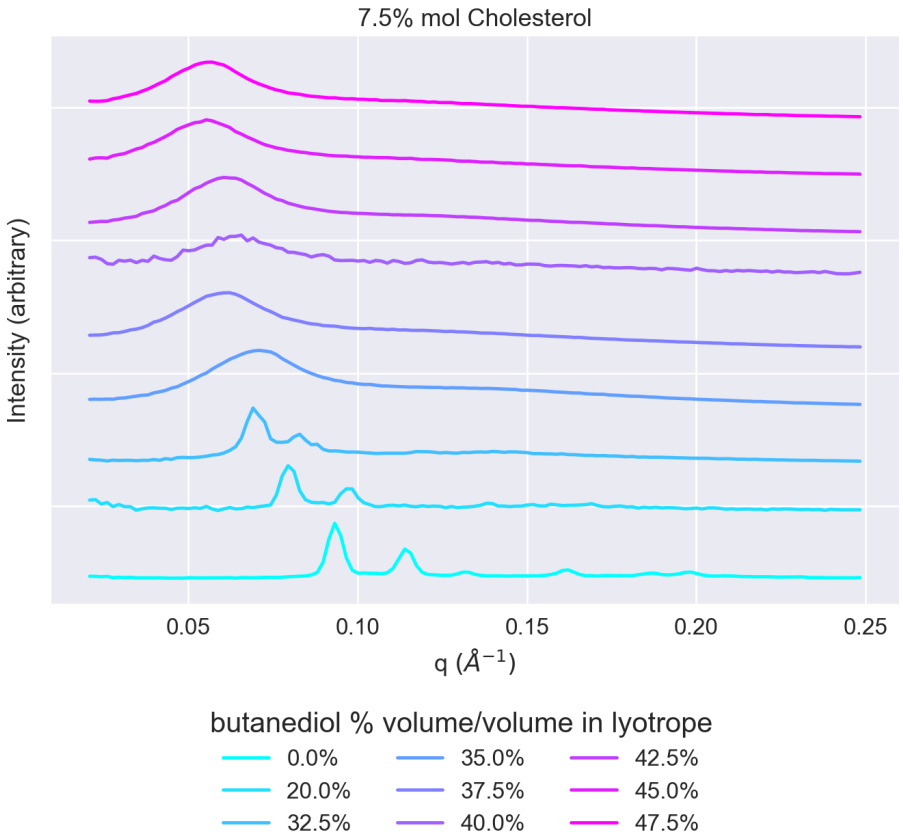

Figure S6: SAXS patterns for systems doped with 7.5% mol cholesterol. The patterns are ordered with increasing butanediol solvent content from bottom to top.

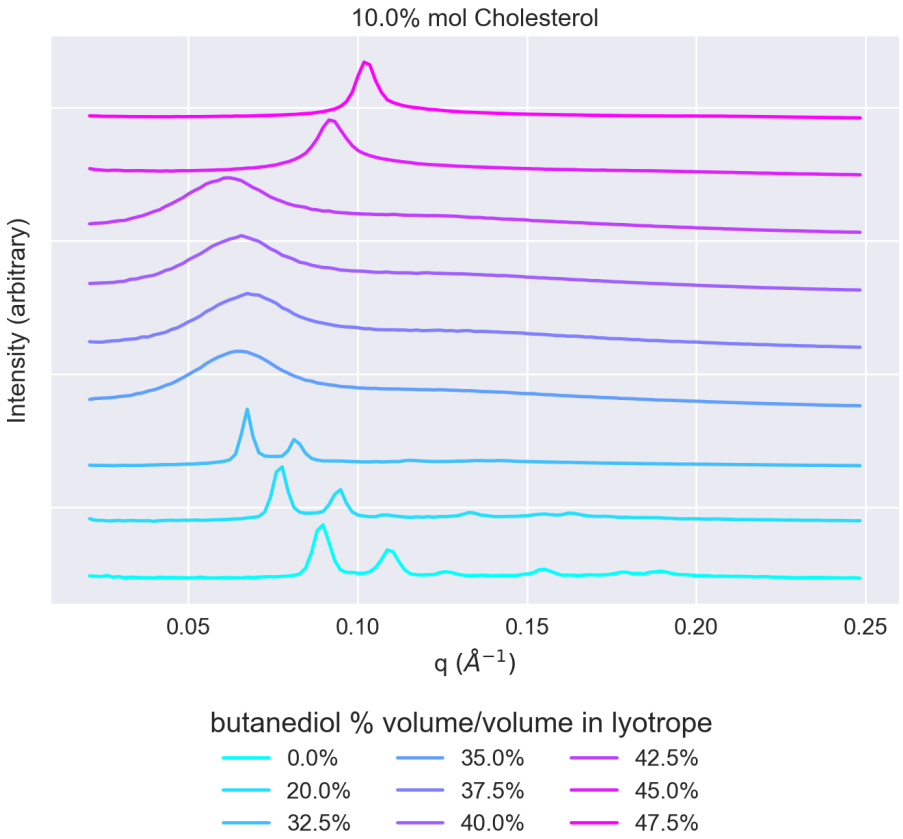

Figure S7: SAXS patterns for systems doped with 10% mol cholesterol. The patterns are ordered with increasing butanediol solvent content from bottom to top.

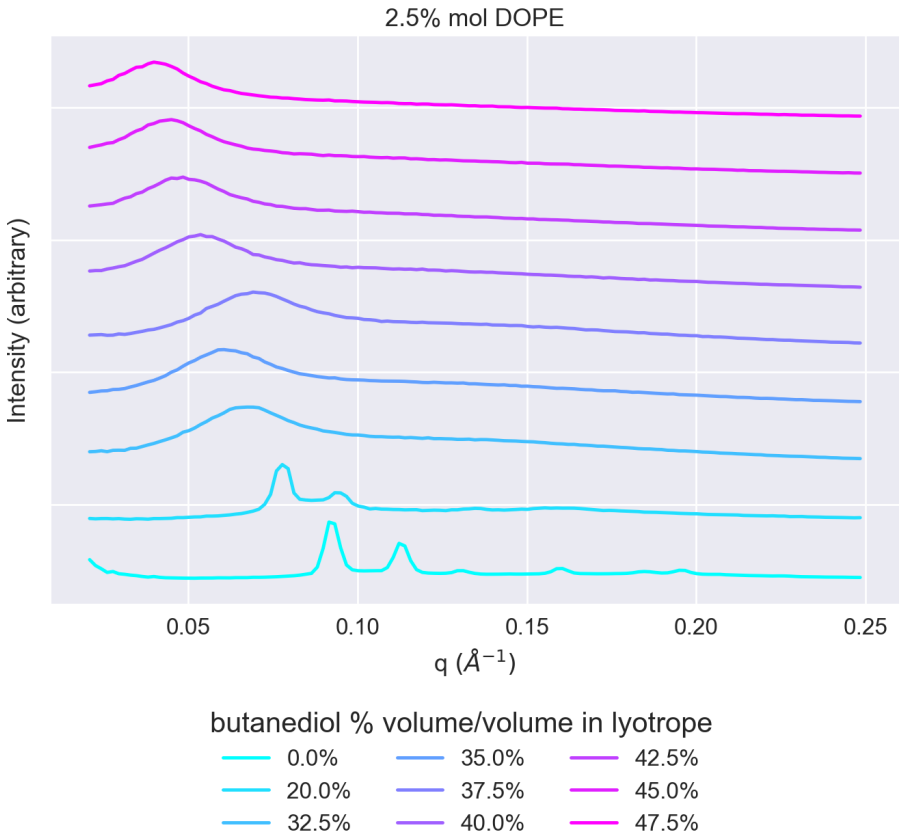

Figure S8: SAXS patterns for systems doped with 2.5% mol DOPE. The patterns are ordered with increasing butanediol solvent content from bottom to top.

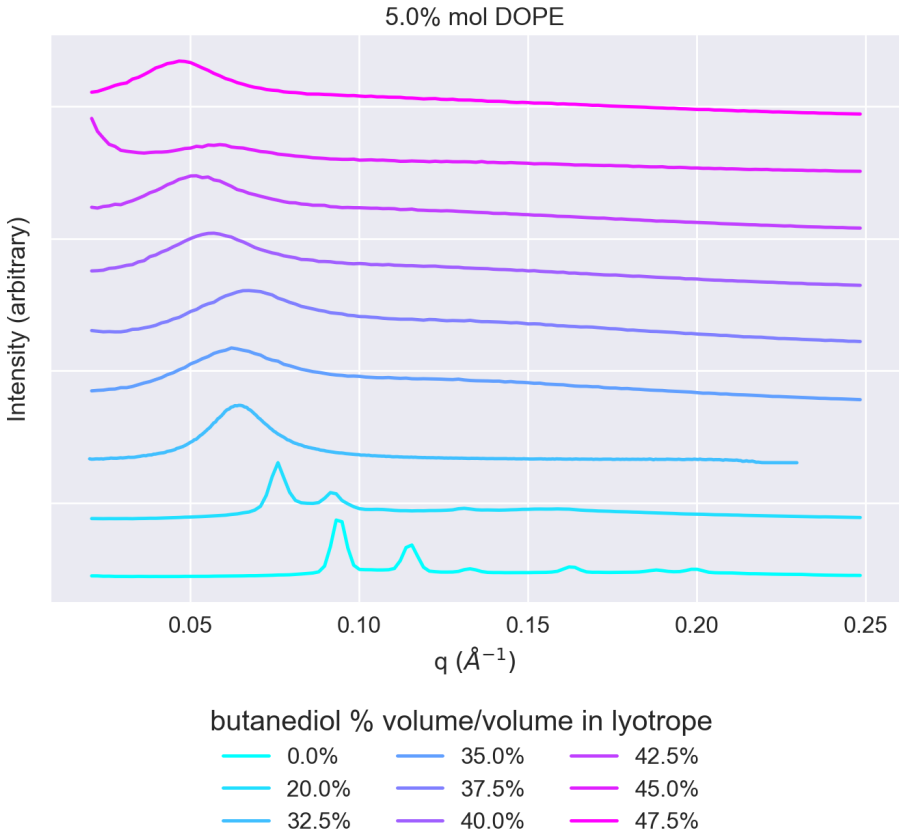

Figure S9: SAXS patterns for systems doped with 5% mol DOPE. The patterns are ordered with increasing butanediol solvent content from bottom to top.

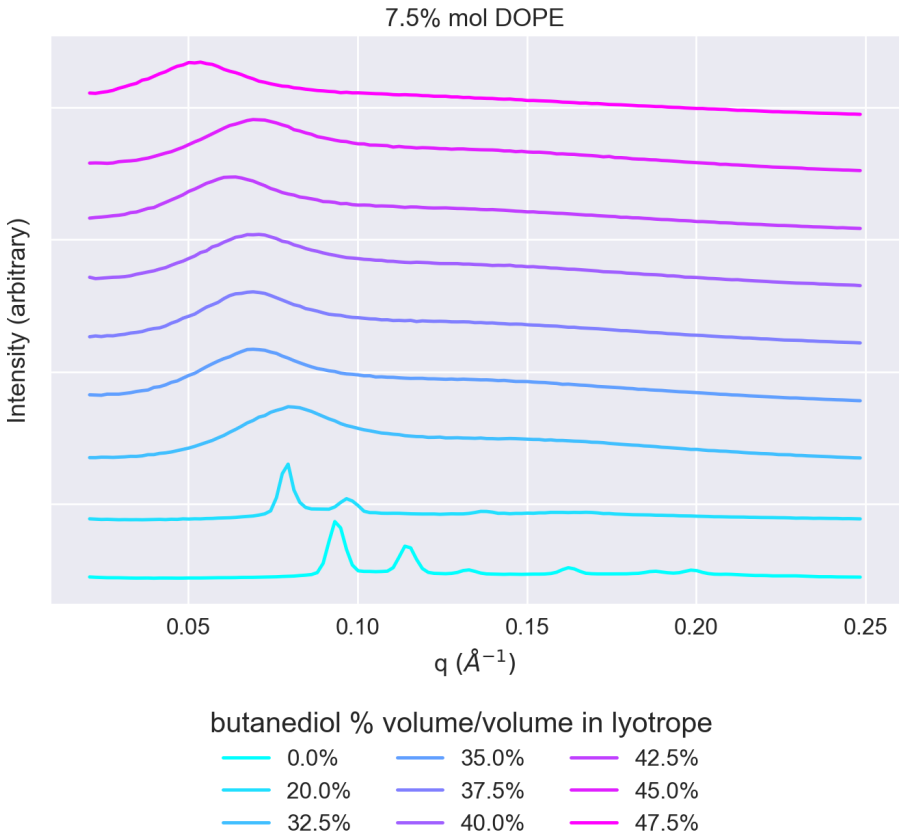

Figure S10: SAXS patterns for systems doped with 7.5% mol DOPE. The patterns are ordered with increasing butanediol solvent content from bottom to top.

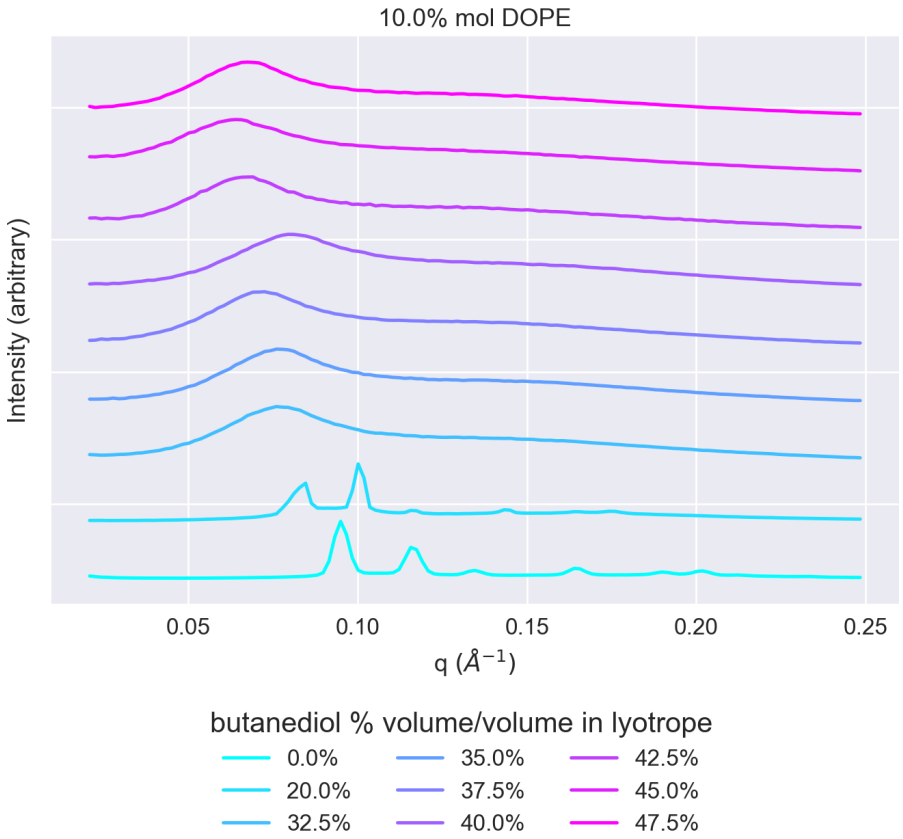

Figure S11: SAXS patterns for systems doped with 10% mol DOPE. The patterns are ordered with increasing butanediol solvent content from bottom to top.

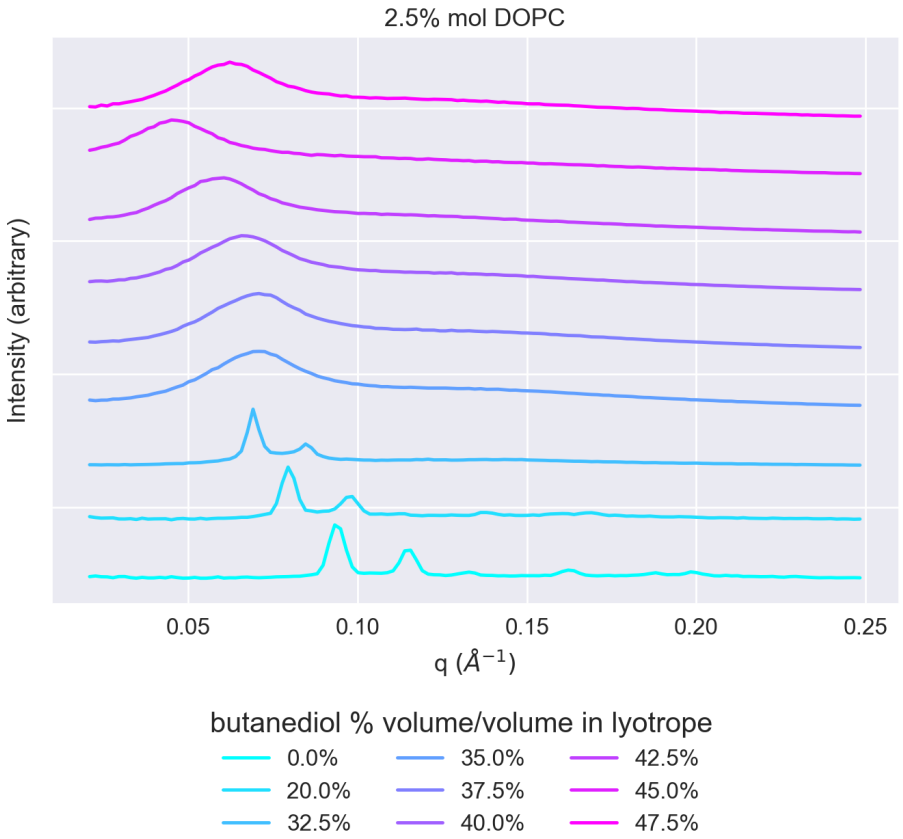

Figure S12: SAXS patterns for systems doped with 2.5% mol DOPC. The patterns are ordered with increasing butanediol solvent content from bottom to top.

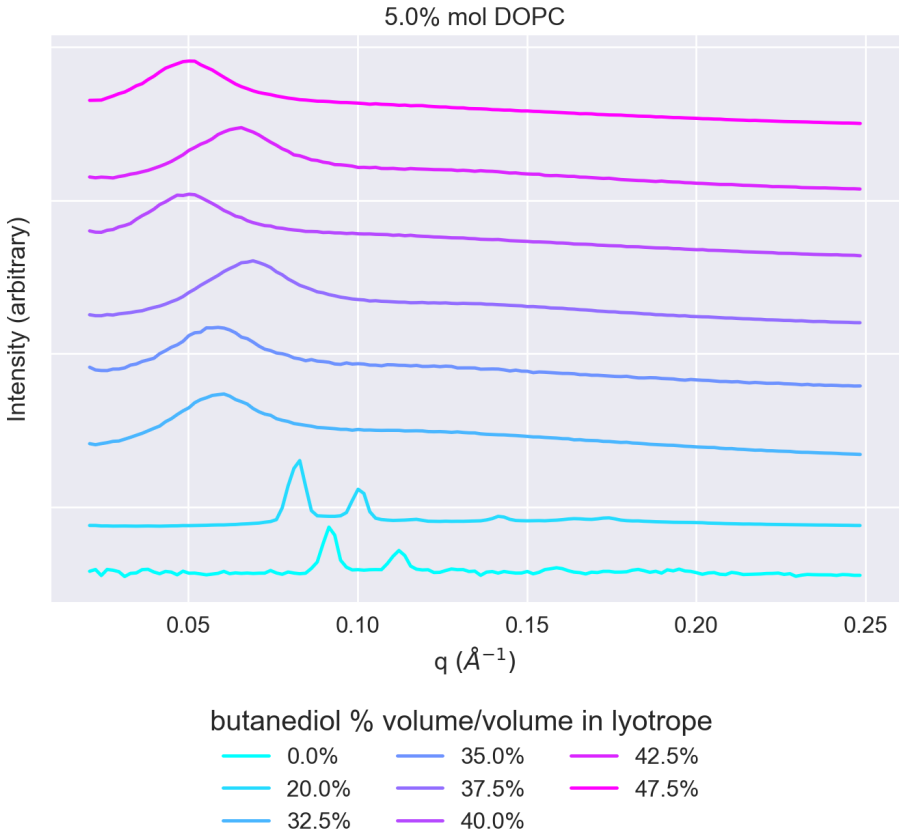

Figure S13: SAXS patterns for systems doped with 5% mol DOPC. The patterns are ordered with increasing butanediol solvent content from bottom to top.

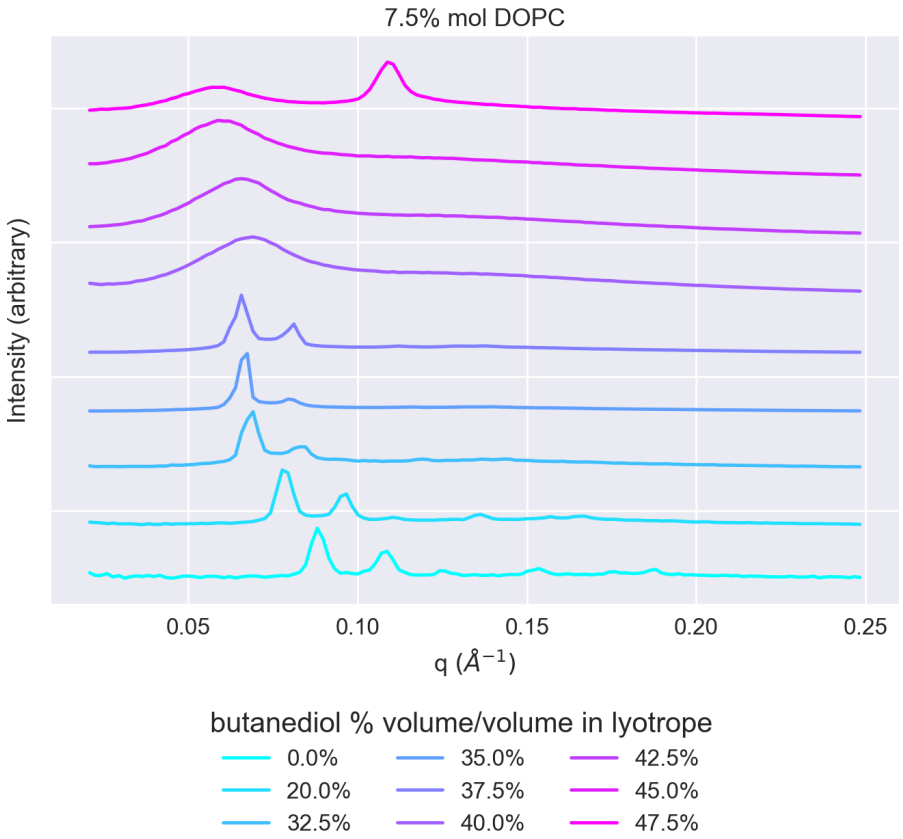

Figure S14: SAXS patterns for systems doped with 7.5% mol DOPC. The patterns are ordered with increasing butanediol solvent content from bottom to top.

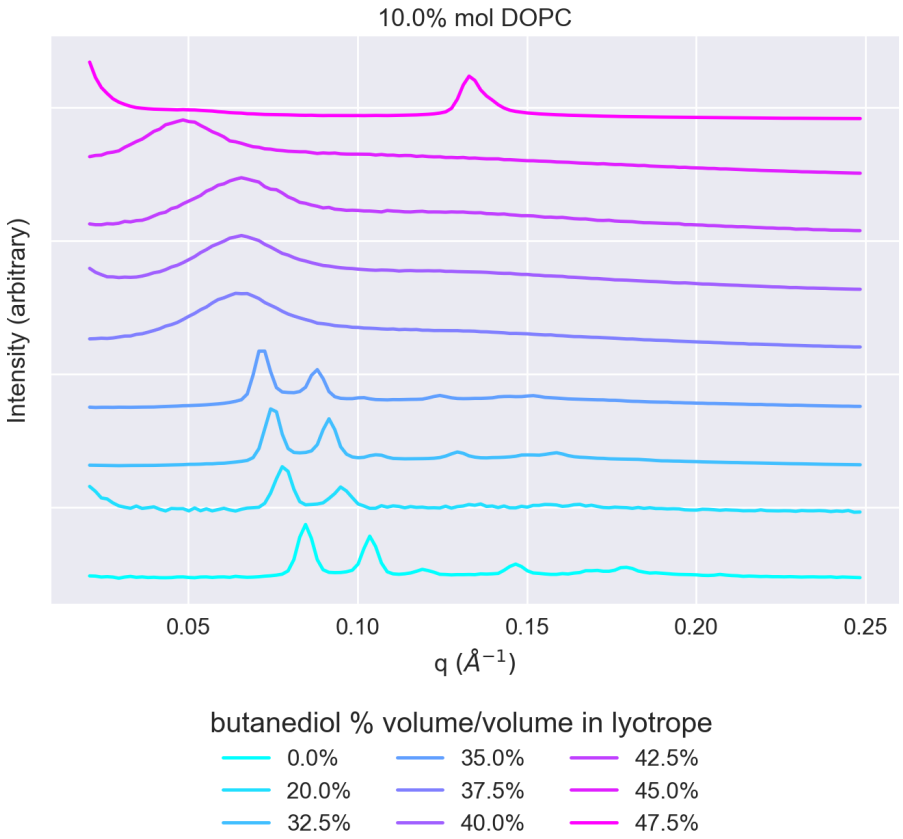

Figure S15: SAXS patterns for systems doped with 10% mol DOPC. The patterns are ordered with increasing butanediol solvent content from bottom to top.

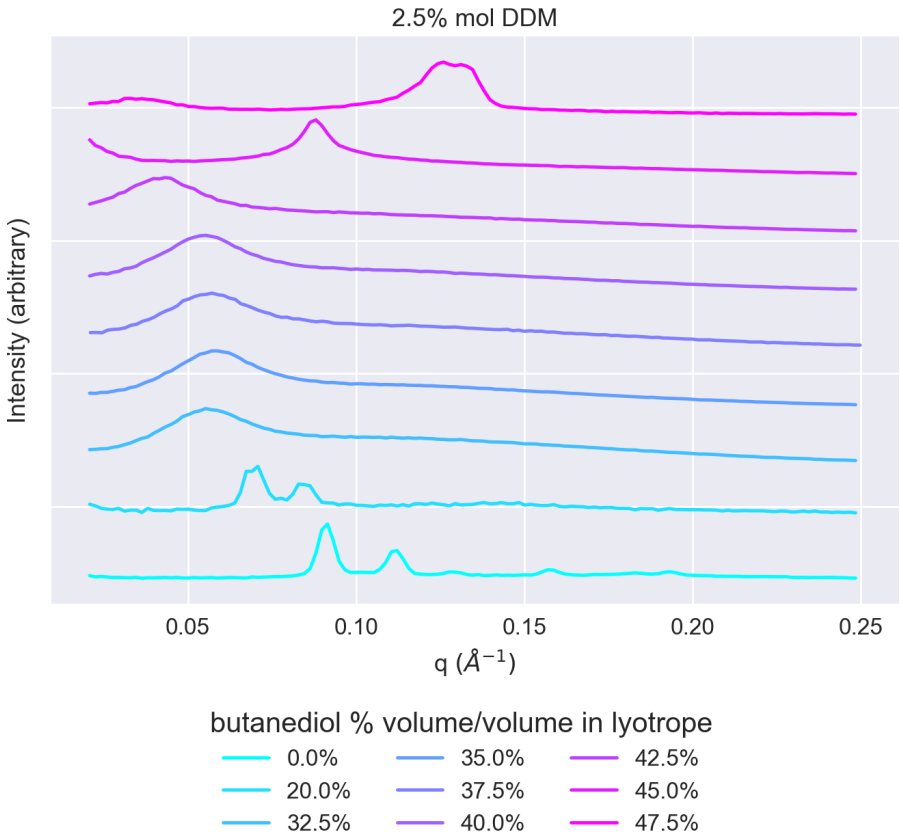

Figure S16: SAXS patterns for systems doped with 2.5% mol DDM. The patterns are ordered with increasing butanediol solvent content from bottom to top.

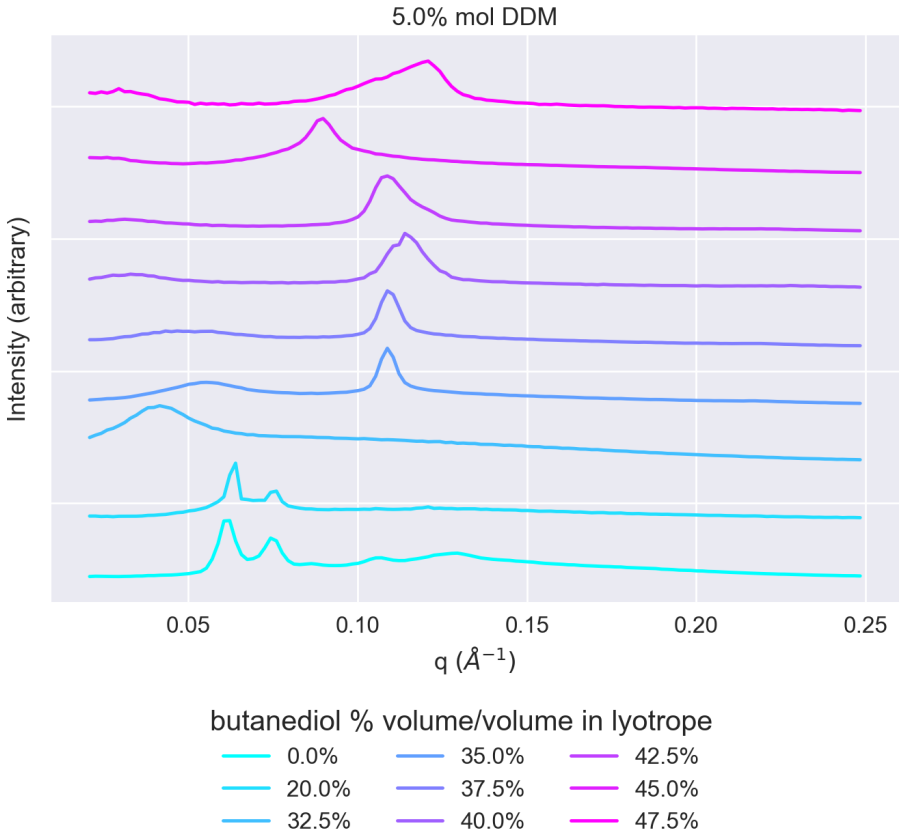

Figure S17: SAXS patterns for systems doped with 5% mol DDM. The patterns are ordered with increasing butanediol solvent content from bottom to top.

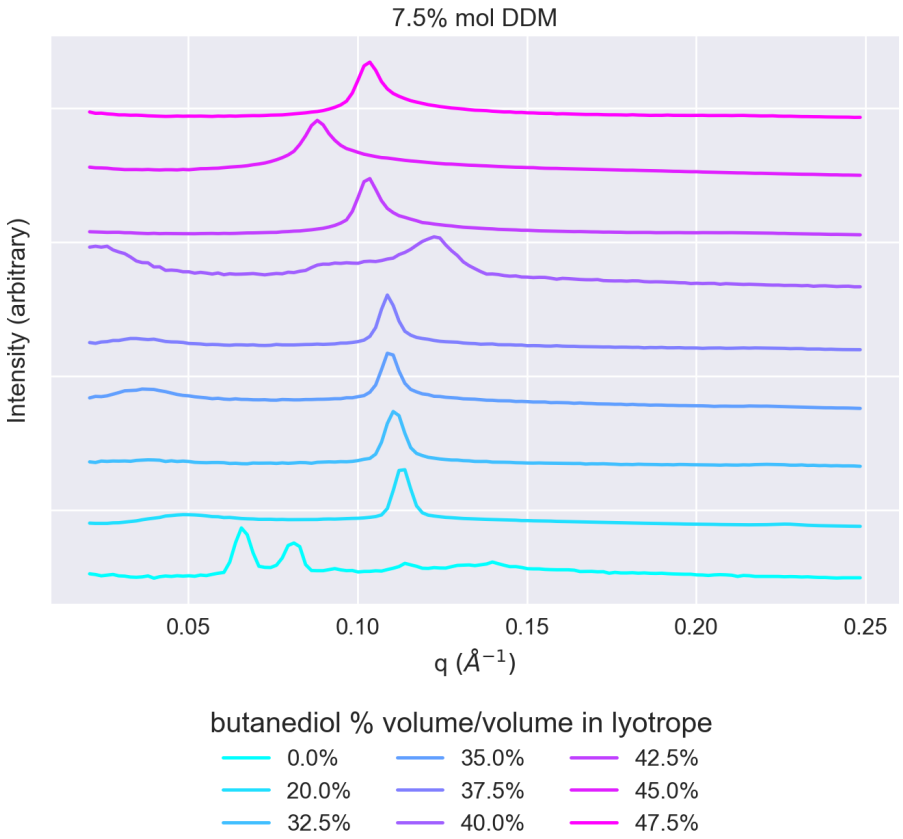

Figure S18: SAXS patterns for systems doped with 7.5% mol DDM. The patterns are ordered with increasing butanediol solvent content from bottom to top.

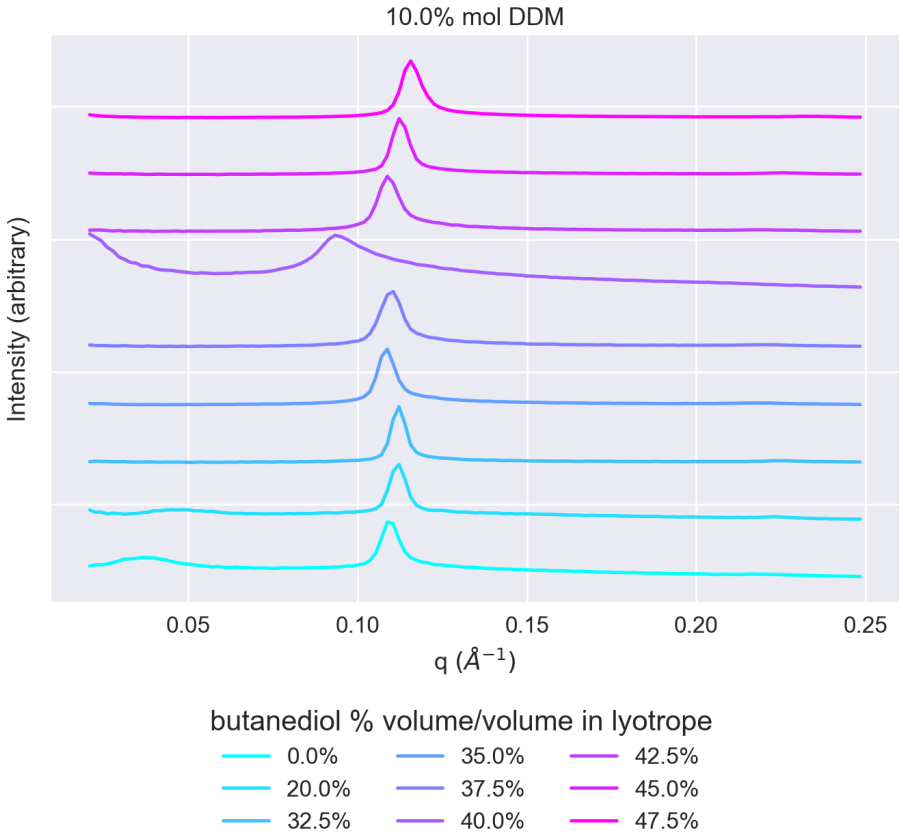

Figure S19: SAXS patterns for systems doped with 10% mol DDM. The patterns are ordered with increasing butanediol solvent content from bottom to top.

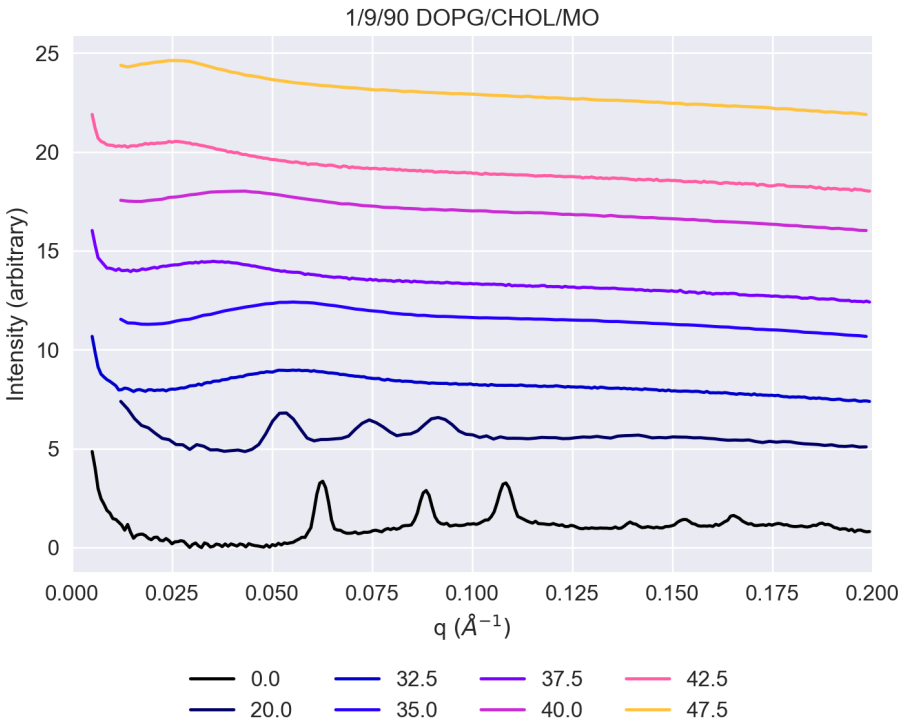

Figure S20: SAXS patterns for systems doped with 1% mol DOPG, 9% mol cholesterol, and 90% mol MO.

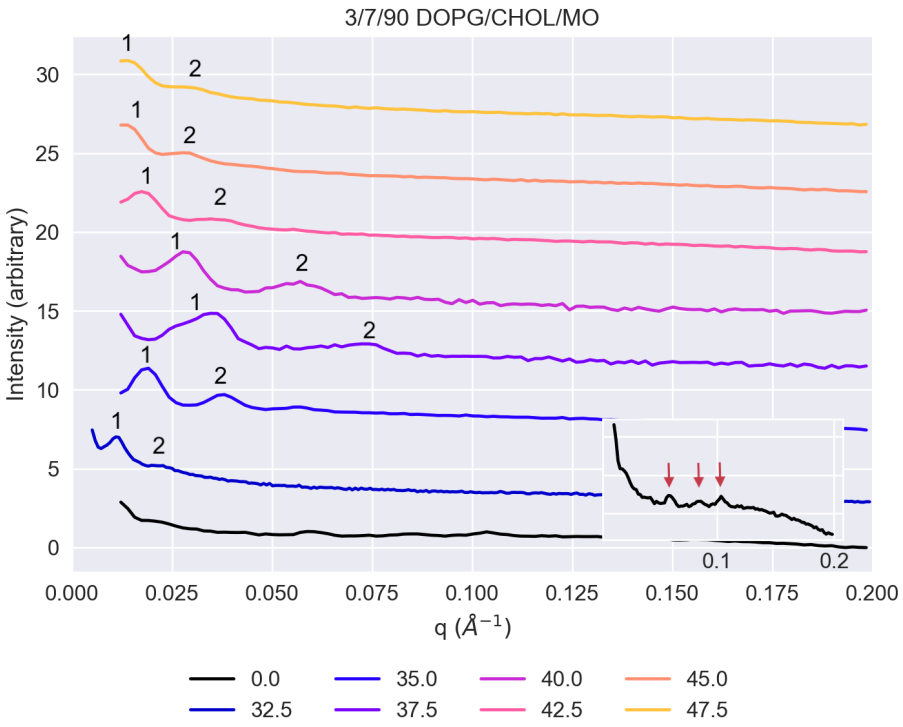

Figure S21: SAXS patterns for systems doped with 3% mol DOPG, 7% mol cholesterol, and 90% mol MO.

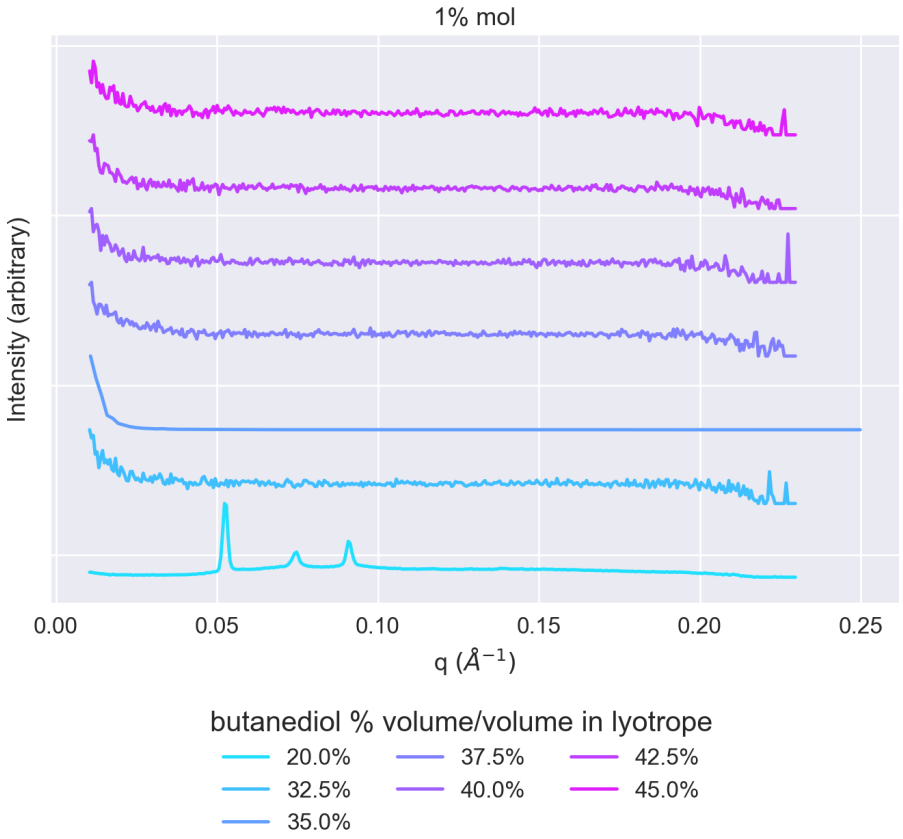

Figure S22: SAXS patterns for systems doped with 1% mol DOPG, and 99% mol MO.

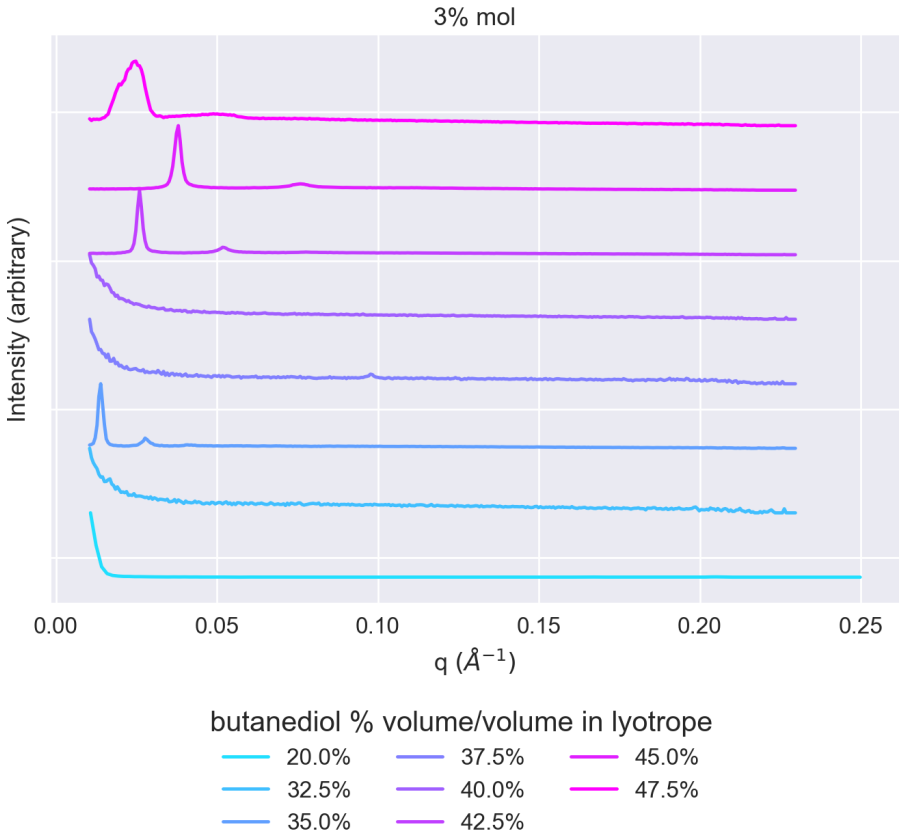

Figure S23: SAXS patterns for systems doped with 3% mol DOPG, and 97% mol MO.

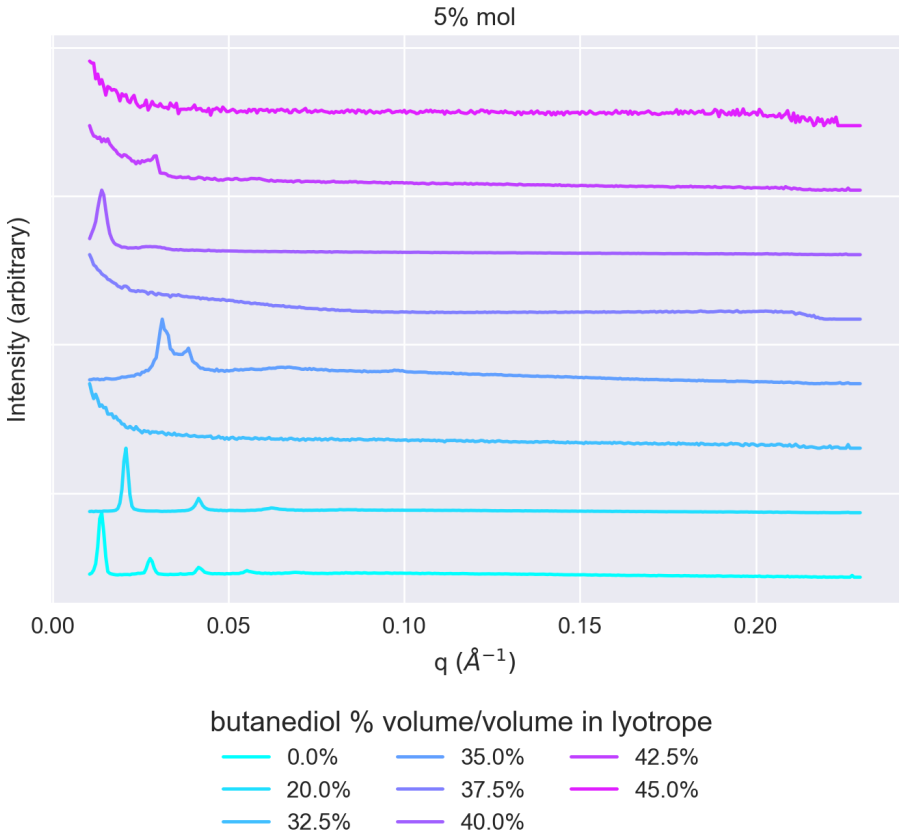

Figure S24: SAXS patterns for systems doped with 5% mol DOPG, and 95% mol MO.

References

[1] G Porte, J Appell, P Bassereau, and J Marignan. Lα to l3 : a topology driven transition in phases of infinite fluid membranes. *Journal de Physique*, 50:1335–1347, 1989. doi: 10.1051/jphys:0198900500110133500ï. URL `http://dx.doi.org/10.1051/jphys:019890050011013350`0.

[2] L. Porcar, W. A. Hamilton, P. D. Butler, and G. G. Warr. Topological relaxation of a shear-induced lamellar phase to sponge equilibrium and the energetics of membrane fusion. *Physical Review Letters*, 93(19), November 2004. doi: 10.1103/physrevlett.93.198301. URL `https://doi.org/10.1103/physrevlett.93.198301`.

[3] Ahanjit Bhattacharya, Henrike Niederholtmeyer, Kira A. Podolsky, Rupak Bhattacharya, Jing-Jin Song, Roberto J. Brea, Chu-Hsien Tsai, Sunil K. Sinha, and Neal K. Devaraj. Lipid sponge droplets as programmable synthetic organelles. *Proceedings of the National Academy of Sciences*, 117(31):18206–18215, July 2020. doi: 10.1073/pnas.2004408117. URL `https://doi.org/10.1073/pnas.2004408117`.

[4] Jan Lipfert, Linda Columbus, Vincent B. Chu, Scott A. Lesley, and Sebastian Doniach. Size and shape of detergent micelles determined by small-angle x-ray scattering. *The Journal of Physical Chemistry B*, 111(43):12427–12438, November 2007. doi: 10.1021/jp073016l. URL `https://doi.org/10.1021/jp073016l`.

[5] Vadim Cherezov, Jeffrey Clogston, Miroslav Z. Papiz, and Martin Caffrey. Room to move: Crystallizing membrane proteins in swollen lipidic mesophases. *Journal of Molecular Biology*, 357(5): 1605–1618, April 2006. doi: 10.1016/j.jmb.2006.01.049. URL `https://doi.org/10.1016/j.jmb.2006.01.049`.